

トピックス

## Edge Radiation from the Fringe Magnetic Fields in Electron Storage Rings

N. V. SMOLYAKOV

*Hiroshima Synchrotron Radiation Center (HSRC), and  
Department of Physical Sciences, Hiroshima University\**

At the present time an edge radiation generated by a relativistic electron beam at fringe fields of bending magnets in storage rings has been the subject of more and more theoretical as well as experimental investigations. The reason is that the edge radiation differ significantly from the well-known standard synchrotron radiation, and its properties are much more attractive for some physical and technical applications than those of synchrotron radiation. An intensive peak appears in the electromagnetic radiation angular distribution in the forward direction at the radiation wavelength well over the synchrotron radiation critical wavelength. Its intensity exceeds considerably the intensity of standard synchrotron radiation. In addition the generation of hard X-rays is suppressed along the straight section axis because the bending magnetic field is depressed at the fringe region. This suggests the use of edge radiation as a good source of infrared, visible or even vacuum ultraviolet radiation. The edge radiation generated at two adjacent edges of bending magnets produces an interference pattern. The real electron beam parameters (its transversal sizes and angular spread) effect on this interference pattern. It provides a way of determining the electron beam parameters from the experimentally measured edge radiation distribution.

### 1. Introduction

Electromagnetic edge radiation (ER) is generated by a relativistic charged particle when it passes through the region of a rapid change in magnetic field at the edges of the storage ring bending magnets. This radiation was experimentally discovered in the late 1970s simultaneously and independently at the Super Proton Synchrotron (SPS, CERN, Geneva, Switzerland)<sup>1-3)</sup> and at the electron synchrotron 'Sirius' (INP, Tomsk, Russia)<sup>4-6)</sup>. A short time after, the ER was observed at the electron synchrotron 'Pakhra' (Moscow, Russia)<sup>7)</sup>.

Theoretically the ER from relativistic proton beam was analysed in papers<sup>8-12)</sup>. In large hadron colliders a short-wavelength ER (with the radiation wavelength  $\lambda \ll \lambda_c$ , where  $\lambda_c$  is the critical wavelength of synchrotron radiation from the uniform magnetic field region of bending magnet) is much more intensive than the standard synchrotron radiation. In view of the fact that in proton storage rings their  $\lambda_c$  correspond to far infrared spectral region<sup>13)</sup>, the proton beam ER manifests itself as a sufficiently intensive visible light, whereas the intensity of proton beam synchrotron radiation in visible spectrum is negligible. The interference pattern produced by the radiation generated at two adjacent edges of different bending magnets was also observed<sup>3)</sup>. This

unique features has enabled ER to be used for proton beam profile measurements at the SPS<sup>2)</sup> and at the TEVATRON at Fermilab<sup>14)</sup>. Similar beam profile monitor is now under consideration in RHIC<sup>13)</sup>.

The ER at electron synchrotron was originally detected in the visible spectral region by M. M. Nikitin<sup>4-6)</sup>. The intensity oscillations in ER spatial distribution due to the interference of radiation generated at two bending magnet fringe fields which set bounds to the same straight section, were observed. The interference pattern changes with the variation both the radiation wavelength and electron beam energy, were also found. Further theoretical investigations of ER generated by a relativistic electron have clearly demonstrated its unique features<sup>15-27)</sup>. The essentials of them are as follows.

In the  $\lambda \gg \lambda_c$  wavelength range an intensive peaks appear in the angular distribution of the ER intensity from a single bending magnet. These peaks exceed considerably the intensity of the standard synchrotron radiation generated in an uniform magnetic field area. Their angular positions do not depend on the radiation wavelength. The peaks of  $\sigma$ -polarised radiation are located in the storage ring median plane at horizontal angles  $\pm \gamma^{-1}$ , where  $\gamma$  is the electron relativistic factor. The peaks of  $\pi$ -polarised radiation are lo-

\* Particle Beam Science Lab., Physical Sciences Dep., Hiroshima University, 1-3-1 Kagamiyama, Higashi-Hiroshima, 739-8526, Japan  
TEL/FAX 0824-24-7489 e-mail nick@sci.hiroshima-u.ac.jp

cated at the angles  $\pm\gamma^{-1}$  above and below the median plane<sup>15-17,23-25,27</sup>).

In the storage ring median plane at horizontal angles  $\pm\gamma^{-1}$ , where the  $\sigma$ -polarised ER peaks are located, the radiation spectrum is long-wavelength shifted and shows a slower decrease with increase in  $\lambda$ <sup>17,23-25</sup>. Since the generation of hard X-rays is suppressed along the straight section because the magnetic field is depressed at fringe regions, undesirable thermal and radioactive damage of optical elements is decreased.

ER generated by a relativistic electron is concentrated in a narrow forward cone. The radiation emitted at two magnetic fringe fields bounding the straight section, appears in the same cone. These photons are subsequently synchronized by the electron itself. This leads to the ER interference effect. The interference manifests itself as additional oscillations in the radiation intensity spatial distribution<sup>10,20,21,24,25</sup>. In view of the fact that the ER spatial distributions, generated at either of the two ends of bending magnets, are generally not trivial, the resulting radiation pattern on the detecting screen is complicated enough. On the other hand, such fine interference structure of resulting ER provides considerable opportunity for the electron beam diagnostics.

The above-listed properties of ER, generated by the relativistic electrons, gave grounds to suggest it as a powerful and bright source of electromagnetic radiation begins with vacuum ultraviolet region and ends with far infrared area<sup>23-25</sup>. The experimental studies of ER intensity, carried out recently in the infrared region, provided support for this view<sup>28</sup>. ER interference pattern is highly irregular in space and depends critically on the electron beam emittance. This provides a means for the electron beam diagnostics with visible ER. Such diagnostic system is used on Siberia-1 electron storage ring (Moscow, Russia)<sup>29,30</sup> and is assumed to be installed at HiSOR electron storage ring (Hiroshima, Japan)<sup>31-33</sup>. However the radiation from quadrupole lenses which are installed into the same straight section makes the interpretation of experimental data far more complicated<sup>34</sup>.

It is interesting to note that the ER by its very nature and spectral properties is very similar to transition undulator radiation<sup>35,36</sup>.

It should be particularly emphasized that the ER generated by the proton beam and the ER generated by the electron beam are an completely different effects although similars in their external manifestations could be found, like the peaks in intensity distributions and the interference effects. Indeed, let us consider a relativistic proton which moves in the straight section exactly along its axis. The ER, generated by this proton, exhibits the increasing of radiation intensity in the short-wavelength spectral region  $\lambda \ll \lambda_c$  (though the short-wavelength radiation means a visible light in the case of proton storage rings). The spatial distribution of the proton's ER has the maximum directed exactly along the straight section axis. From the theoretical standpoint, the ER generated by a relativistic proton belongs to the category of so-called dipole-type radiation. This is due to the fact that the typical length of synchrotron radiation generation  $\rho_0/\gamma$ ,

which is of the order of several meters, is many times longer than the length of bending magnet fringe field, which is of the order of 10 cm or shorter. Here  $\rho_0$  is the proton's orbit bending radius. The last-mentioned property makes it feasible to derive the reasonably simple analytical formulae for the spectral-angular distributions of dipole ER<sup>9-12</sup>. These formulae show in an explicit form that the ER spectrum is highly sensitive to the fringe field shape. Consequently, in this case the step-function is unusable as an approximation for the fringe field.

As is evident from the foregoing the ER generated by the relativistic electron, has another spectral distribution ( $\lambda \gg \lambda_c$ ) and another angular positions of its peaks:  $\pm\gamma^{-1}$  apart from the straight section axis. Among other things, this radiation is not dipole-type radiation since the magnitude  $\rho_0/\gamma$ , which is of the order of millimeter or even less in the electron storage rings, is many times shorter than the length of bending magnet fringe field. It means that computer simulations must be carried out to get the reliable theoretical results. Some simple analytical formulae were derived in<sup>17,18,25,27</sup> within the long-wavelength approximation limit  $\lambda \rightarrow \infty$ . The last mentioned approach restricts considerably the practical usage of the derived formulae.

It may be said in summary that the availability of straight sections in the high-energy storage rings tends to increase the intensity of the long-wavelength radiation ( $\lambda \gg \lambda_c$ ). It has been just this effect which is referred to as the ER from an electron beam. Strictly speaking, such type effect will also be available in a proton storage rings with a straight sections. In this case, this effect will exhibit itself as the increasing of radiation intensity at radio-wavelengths range and is of no practical significance. If the bending magnets, in addition, have the short fringe field lengths (shorter, than  $\rho_0/\gamma$ ), so the intensity of short-wavelength radiation ( $\lambda \ll \lambda_c$ ) will be enlarged also. This effect manifests itself as ER from a relativistic proton beam. Usually, a bending magnets have the short fringe field lengths as related to the magnitude  $\rho_0/\gamma$  at the proton storage rings and never have the short fringe fields at the electron storage rings. That is why there is no increase of the short-wavelength radiation intensity along the electron storage rings straight sections. In contrast, the short-wavelength radiation intensity will be suppressed in this case. It should be noted in this connection that the results, obtained in paper<sup>37</sup>, contrary to its title, can be used to the proton beams (and as a crude approximation only) rather than to the electron beams.

The currently available experimental data about the ER properties, generated by relativistic electron beam, are few in number and are listed in references. This paper presents the theoretical investigations of ER. Some formulae which describe the ER properties in general case are presented in chapter 2. The computer simulated ER distributions are presented in chapter 3. The simulations were made for the HiSOR storage ring (Hiroshima, Japan)<sup>38-41</sup> with electron beam energy 0.7 GeV. The simple analytical formulae which can be used for the long-wavelength ER analysis are derived in chapter 4. The features of ER properties in long-

wavelength region are discussed therein. The advantages of the ER applications for electron beam diagnostics are briefly discussed in chapter 5.

## 2. Electromagnetic radiation from relativistic electron in planar fields

Let us consider a relativistic electron moves along the trajectory  $\vec{r}(t)$ . Let  $\vec{\beta}$ ,  $\dot{\vec{\beta}}$  and  $\gamma$  are the reduced velocity, acceleration and energy of this electron. The equation of motion for the electron in the external magnetic field  $\vec{H}(\vec{x})$  is:

$$\dot{\vec{\beta}}(t) = \frac{e}{mc\gamma} \vec{\beta}(t) \times \vec{H}(\vec{r}(t)), \quad (1)$$

where  $e$  and  $m$  are the electron charge and mass,  $c$  is the speed of light.

At the observation point  $\vec{x}^*$  and at the observation time  $\tau$  the electric field vector of the radiation emitted by an electron is given by the formula

$$\begin{aligned} \vec{E}(\tau) = & \frac{e}{cR(t)} \frac{\vec{n}(t) \times (\vec{n}(t) - \vec{\beta}(t)) \times \dot{\vec{\beta}}(t)}{(1 - \vec{n}(t) \cdot \vec{\beta}(t))^3} \\ & + \frac{e}{R^2(t)\gamma^2} \frac{\vec{n}(t) - \vec{\beta}(t)}{(1 - \vec{n}(t) \cdot \vec{\beta}(t))^3}, \end{aligned} \quad (2)$$

where the unit vector  $\vec{n}(t)$  points from the electron to the observer, which are separated by the distance  $R(t)$ :  $\vec{R}(t) = \vec{x}^* - \vec{r}(t)$ ,  $\vec{n}(t) = \vec{R}(t)/R(t)$ . The quantities  $\vec{n}$ ,  $\vec{\beta}$ ,  $\dot{\vec{\beta}}$  and  $R$  on the right-hand side of Eq. (2) are to be evaluated at the time  $t$ :

$$\tau = t + R(t)/c. \quad (3)$$

The first and second terms in (2) are the radiation and Coulomb fields respectively. Usually the Coulomb term is negligibly small and will be further ignored.

The spectral-angular properties of electromagnetic radiation with frequency  $\omega$  are determined by Fourier-transform of electric field:

$$\vec{E}(\omega) = \int_{-\infty}^{\infty} e^{i\omega\tau} \vec{E}(\tau) d\tau. \quad (4)$$

Let the  $Y$ -axis of Cartesian coordinates be aligned with the straight section axis and  $Z$ -axis be directed vertically. It is convenient to set the intersection point of the electron beam equilibrium trajectory with the fringe field of the first bending magnet BM1 as the origin of coordinates (see Fig. 1). Let  $y_1$  be the initial point of the bending magnet BM1 field. In the storage ring median plane  $xOy$  (i.e.  $z=0$ ) magnetic field of the bending magnet BM1 is directed vertically and is given by the function  $H_0 h(y)$ , where  $H_0$  is the uniform magnetic field amplitude and  $h(y)$  describes the shape of magnetic field:  $h(y < y_1) = 0$ ,  $h(+\infty) = 1$ . Let  $y_2$  be the terminal point of the bending magnet BM2 field, so that the points  $y_1$  and  $y_2$  are symmetric to each other about the straight section

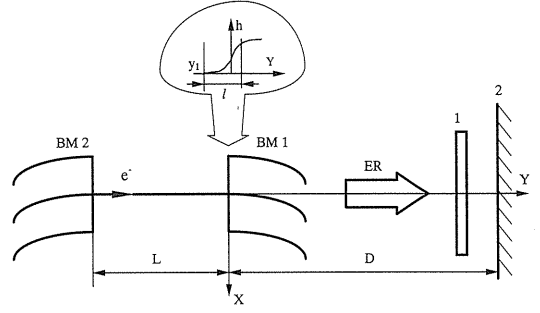


Figure 1. Edge radiation detection scheme: 1-band-pass filter, 2-detector screen.

center, the point  $0.5(y_1 + y_2)$  is the straight section center and  $L = y_1 - y_2$  is the straight section length. The resulting magnetic field produced by two bending magnets in the neighbourhood of a straight section is suggested to be symmetric about the straight section center and therefore is equal to:

$$H(y) = H_0(h(y) + h(y_1 + y_2 - y)). \quad (5)$$

Let a relativistic electron travels at the straight section center exactly along the positive  $Y$  axis. Let this electron was at the point  $y_2$  at the instant  $t_2$  and subsequently at the point  $y_1$  at the instant  $t_1$ :  $r_y(t_1) = y_1$ ,  $r_y(t_2) = y_2$ .

It is readily available from (3) that  $(d\tau/dt) = 1 - (\vec{n}(t) \cdot \dot{\vec{\beta}}(t))$ , and hence:

$$\tau(t) = \tau(t_1) + \int_{t_1}^t (1 - (\vec{n}(t') \cdot \dot{\vec{\beta}}(t'))) dt'. \quad (6)$$

Substituting of (2) and (6) into Eq. (4), neglecting by Coulomb term and changing the integration with respect to variable  $\tau$  by the integration with respect to variable  $t$ , we have:

$$\vec{E}(\omega) = \vec{E}_1(\omega) + \vec{E}_2(\omega), \quad (7)$$

$$\begin{aligned} \vec{E}_1(\omega) = & \frac{e}{c} \int_{t_1}^{\infty} \frac{\vec{n}(t) \times (\vec{n}(t) - \vec{\beta}(t)) \times \dot{\vec{\beta}}(t)}{R(t)(1 - \vec{n}(t) \cdot \vec{\beta}(t))^2} \\ & \times \exp(i\omega\tau(t)) dt, \end{aligned} \quad (8)$$

$$\begin{aligned} \vec{E}_2(\omega) = & \frac{e}{c} \int_{-\infty}^{t_2} \frac{\vec{n}(t) \times (\vec{n}(t) - \vec{\beta}(t)) \times \dot{\vec{\beta}}(t)}{R(t)(1 - \vec{n}(t) \cdot \vec{\beta}(t))^2} \\ & \times \exp(i\omega\tau(t)) dt. \end{aligned} \quad (9)$$

The terms  $\vec{E}_1(\omega)$  and  $\vec{E}_2(\omega)$  describe the ER from the first magnet BM1 and from the second magnet BM2 respectively.

Let  $\vec{k}$  be the vertically directed (along  $z$ -axis) unit vector, vectors  $\vec{e}_\sigma$  and  $\vec{e}_\pi$  are the unit vectors of radiation polarization. This polarization vectors are defined as follows (recall that the vector  $\vec{x}^* = \{x^*, D, z^*\}$  starts at the origin of the coordinates and ends at the observation point):

$$\bar{e}_\sigma = \frac{\bar{k} \times \bar{x}}{|\bar{k} \times \bar{x}|}, \quad (10)$$

$$\bar{e}_\pi = \bar{x} \times \bar{e}_\sigma. \quad (11)$$

Vectors  $\bar{e}_\sigma$  and  $\bar{e}_\pi$  correspond to the horizontal and vertical components for the electrical field respectively.

The most commonly used convention employs the spectral-angular distribution of the emitting radiation energy, which is given by the next expression:

$$\frac{d\varepsilon}{d\Omega d\omega} = \frac{cR^2}{4\pi^2} |\tilde{E}(\omega)|^2. \quad (12)$$

By this is meant that the observer is placed infinitely far from the region where the radiation is emitted. The real geometry of any physical experiment implies that all the distances are finite. Moreover, the distance to the observer may be of the order of the straight section length. The near field effects<sup>42)</sup> must be included into consideration in this case. It means that the  $t$ -dependence of the unit vector  $\bar{n}$  should be taken into account. That is why we will consider the number of photons which reach an infinitesimally small element of a plane  $ds$  placed normally to the  $Y$ -axis at the observation point  $\bar{x}^*$ . For practical purposes, it will be also much more convenient to consider the number of photons  $dN/dt$  which are generated by the electron beam per second. We will consider the single-particle approximation in this chapter, i.e. we assume the electron beam to be with zero emittance, non-bunched and to move in the storage ring median plane along the  $Y$ -axis. The effect of the real beam emittance on the electromagnetic radiation distributions will be discussed in chapter 5. The different electrons in such a beam generate the radiation incoherently, so that the radiation characteristics of such zero-emittance beam is definite by that of a single electron. As a result, we have the next expression for the number of photons generated by the zero-emittance electron beam per second:

$$\frac{dN_{\sigma,\pi}}{dt} = ds \left( \frac{d\omega}{\omega} \right) \left( \frac{I}{e} \right) \frac{\alpha c^2}{4\pi^2 e^2} |\tilde{E}_{\sigma,\pi}(\omega)|^2, \quad (13)$$

where  $I$  is the electron beam current,  $\alpha$  is the fine structure constant.

Since there is a one-to-one correspondence between the electron's longitudinal coordinate  $y$  and time  $t$ , we will use variable  $y$  instead of time  $t$  in the electron trajectory description. In other words, we will consider time  $t$  as a formal function of the electron's longitudinal coordinate  $y$ :  $t=t(y)$ . In this case the formulae for the electron's trajectory have the forms:

$$\bar{\beta}(y) = \{\beta_x(y), \sqrt{\beta^2 - \beta_x^2(y)}, 0\}, \quad \bar{r}(y) = \{r_x(y), y, 0\}.$$

First we consider the term  $\tilde{E}_1(\omega)$  which presents an ER from the first bending magnet BM1. It is straightforward to show from (1) that at  $y_1 < y$ :

$$\beta_x(y) = -\frac{\delta}{\rho_0} \int_{y_1}^y h(y') dy', \quad (14)$$

$$r_x(y) = \int_{y_1}^y \beta_x(y') dy', \quad (15)$$

where  $\rho_0 = (mc^2\gamma / |eH_0|)$  is the electron orbit radius in the bending field,  $\delta = \text{sign}(H_0) = \pm 1$ . In the neighbourhood of a straight section where the ER is produced, the bending magnetic field deflects the electron through a small angle:  $|\beta_x(y)| \ll 1$ .

Let  $\xi$  and  $\zeta$  be the horizontal and vertical angular coordinates of an observation point  $\bar{x}^*$  respectively, i.e.  $\xi = (x^*/D)$ ,  $\zeta = (z^*/D)$ . Usually both straight section length  $L$  and distance to the observer  $D$  are much longer than the fringe field length  $l$ . It means that the next approximations are valid at  $y_1 < y$ :

$$n_x(y) \cong \xi, \quad n_z(y) \cong \zeta.$$

One can readily be obtained for the small observation angles  $|\xi| \ll 1$ ,  $|\zeta| \ll 1$  that

$$\frac{\bar{n}(y) \times [(\bar{n}(y) - \bar{\beta}(y)) \times [\bar{\beta}(y) \times \bar{k}]]}{2\gamma^2(1 - \bar{n}(y) \cdot \bar{\beta}(y))^2} = f_\sigma(y)\bar{e}_\sigma + f_\pi(y)\bar{e}_\pi, \quad (16)$$

$$f_\sigma(y) = \frac{1 - \gamma^2(\xi - \beta_x(y))^2 + \gamma^2\zeta^2}{[1 + \gamma^2(\xi - \beta_x(y))^2 + \gamma^2\zeta^2]^2}, \quad (17)$$

$$f_\pi(y) = \frac{2\gamma^2(\xi - \beta_x(y))\zeta}{[1 + \gamma^2(\xi - \beta_x(y))^2 + \gamma^2\zeta^2]^2}, \quad (18)$$

$$\omega\tau(t(y)) = \Phi(y) + \Phi_0, \quad (19)$$

$$\Phi(y) = \frac{\pi}{\lambda\gamma^2} \left[ (1 + \gamma^2\xi^2 + \gamma^2\zeta^2)(y - y_1) - 2\gamma^2\xi r_x(y) + \gamma^2 \int_{y_1}^y \beta_x^2(y') dy' \right], \quad (20)$$

where  $\lambda$  is the radiation wavelength. The functions  $\beta_x(y)$  and  $r_x(y)$  are given in (14) and (15). The expressions (19) and (20) are readily calculated from relation (6). The phase term  $\Phi_0$  being independent on the longitudinal coordinate  $y$ , is isolated in (19) from the main phase term  $\Phi(y)$ .

We can conveniently define two non-dimensional functions:

$$F_{\sigma,\pi}(\xi, \zeta) = \frac{\gamma\delta}{\rho_0} \int_{y_1}^{\infty} \exp(i\Phi(y)) f_{\sigma,\pi}(y) h(y) dy. \quad (21)$$

Using the relations obtained above, it can be shown from (8) that:

$$\tilde{E}_{1\sigma,\pi}(\omega) = \frac{2|e|\gamma}{cD} F_{\sigma,\pi}(\xi, \zeta). \quad (22)$$

In perfect analogy to the preceding analysis, it can be ob-

tain from (9) that:

$$\tilde{E}_{2\sigma,\pi}(\omega) = \frac{2|e|\gamma}{c(D+L)} \bar{F}_{\sigma,\pi}(-\xi_2, -\zeta_2) \exp(-i\Delta\Phi), \quad (23)$$

where  $\xi_2 = (x^*/(D+L))$  and  $\zeta_2 = (z^*/(D+L))$  are the horizontal and vertical angles respectively, at which an observation point  $\bar{x}^*$  is viewed by the electron while it is located at the end of second magnet BM2. For simplicity the same phase factor is omitted in (22) and (23). The horizontal line at the top of (23) means complex conjugation, the additional phase  $\Delta\Phi$  corresponds to the electron passage within the straight section length:

$$\Delta\Phi = \frac{\pi L}{\lambda\gamma^2} \left[ 1 + \gamma^2(\xi^2 + \zeta^2) \frac{D}{D+L} \right]. \quad (24)$$

Relations (22) and (23) state that the properties of radiation generated at two edges of different bending magnets are related to each other. Formally the functions  $F_{\sigma,\pi}(\xi, \zeta)$  determine the ER properties from the first bending magnet only because the integration in (21) is performed only over the region of the first bending magnet. But the relation (23) shows that at the same time functions  $F_{\sigma,\pi}(\xi, \zeta)$  determine the properties of the ER from the second bending magnet also.

As a result, we have the following expressions for the number of photons generated by the electron beam per second:

$$\frac{dN_{\sigma,\pi}}{dt} = ds \left( \frac{d\omega}{\omega} \right) \left( \frac{I}{e} \right) \frac{\alpha\gamma^2}{\pi^2} \left| \frac{1}{D} F_{\sigma,\pi}(\xi, \zeta) + \frac{\exp(-i\Delta\Phi)}{D+L} \bar{F}_{\sigma,\pi}(-\xi_2, -\zeta_2) \right|^2. \quad (25)$$

The first  $F_{\sigma,\pi}$  and second  $\bar{F}_{\sigma,\pi}$  terms in (25) correspond to the ER, generated by the electron beam at the first BM1 and at the second BM2 bending magnets respectively. Taking into consideration both these terms, we will get the interference effect due to the phase factor  $\exp(-i\Delta\Phi)$ .

It must be emphasized that the all approximations were made above are caused only by the small observation angles  $|\xi| \ll 1$ ,  $|\zeta| \ll 1$  and high electron energy  $\gamma \gg 1$ . Excepting this two limitations, mentioned immediately above, all formulae obtained in this chapter are general enough. In the particular case of dipole-type ER, when the length of fringe field  $l$  is much shorter than the magnitude  $\rho_0/\gamma$ , and in the short-wavelength region  $\lambda \ll \lambda_c$  this formulae may be significantly simplified to the coincidence with results obtained in Refs. 9–11.

At the end of this chapter we present without proof the formula for the angular distribution of the radiation power, i.e. integrated over all the wavelengths spectral-angular distribution of the electromagnetic radiation energy:

$$\frac{dW}{d\Omega} = \frac{2e^4\gamma^4}{\pi m^2 c^4} \left( \frac{I}{e} \right) \int_{-\infty}^{\infty} H^2(y)$$

$$\times \frac{[1 + \gamma^2(\xi - \beta_x(y))^2 + \gamma^2\zeta^2]^2 - 4\gamma^2(\xi - \beta_x(y))^2}{[1 + \gamma^2(\xi - \beta_x(y))^2 + \gamma^2\zeta^2]^5} dy. \quad (26)$$

It is suggested for the sake of simplicity that the observation point is located infinitely far from the storage ring.

### 3. Computation results

The computer simulations presented below were made for the HiSOR storage ring<sup>38-41</sup>. For simplicity the observation point was placed infinitely far from the bending magnets. The following HiSOR storage ring parameter were used in the simulations: the electron beam energy is 0.7 GeV, the beam current is 300 mA, the bending magnetic field is 2.7 T, the distance between magnets  $L$  is 8240 mm,  $\lambda_c = 1.42$  nm (critical energy is 873 eV). In the computations having been made the  $h(y)$  function descriptive the fringe field shape and measured in the real bending magnet of HiSOR storage ring was used. The manufacturer of the accelerator system is Sumitomo Heavy Industries, Ltd. The fringe magnetic field measurements were made in the same institute. The result of this measurements is shown in Fig. 2.

Fig. 3 shows the horizontal distribution of the ER intensity in  $phot/mrad^2/s/(0.1\%BW)$  with different photon energies: 5, 2, 0.5 and 0.05 eV, generated at the first bending magnet BM1. Radiation supposed to be observed at the storage ring median plane. The standard synchrotron radiation is associated with large horizontal angle  $\xi \gg \gamma^{-1} = 0.73$  mrad, at the right of Fig. 3. On can see that starting from vacuum ultraviolet radiation region, an intensive peak located at  $\xi = \gamma^{-1}$  appears in the ER horizontal angular distribution. On further wavelength rising the second peak appears at  $\xi = -\gamma^{-1}$ . This peaks becomes approximately symmetrical with the further wavelength increase, and the correspondent radiation intensity considerably exceed that of the conventional synchrotron radiation. It is in agreement with the ER asymptotic analysis<sup>16,18</sup> in the long-wavelength limit  $\lambda \rightarrow \infty$ . There are no peaks at  $\lambda \leq \lambda_c$ , the intensity of radiation at small angles  $|\xi| < 2\gamma^{-1}$  is below the intensity level of the conventional synchrotron radiation. This is evident from Fig. 4, where the normalized horizontal distributions of power (in

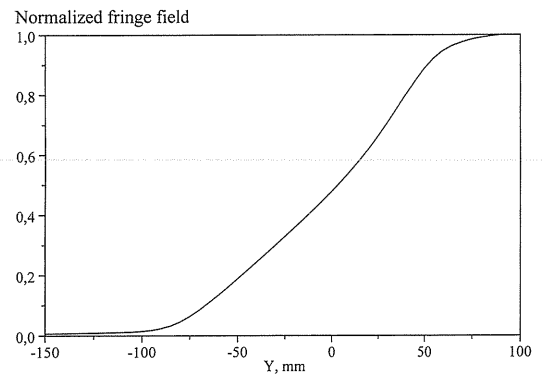


Figure 2. Normalized magnetic field at the bending magnet edge of HiSOR storage ring.

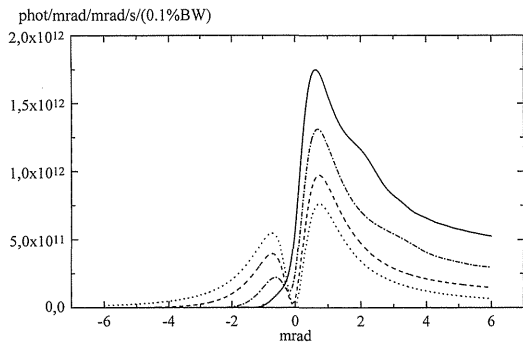


Figure 3. Horizontal distributions of the edge radiation in the median plane for the different photon energy: 5 eV-solid line, 2 eV-dot-dashed line, 0.5 eV-dashed line, 0.05 eV-dotted line.

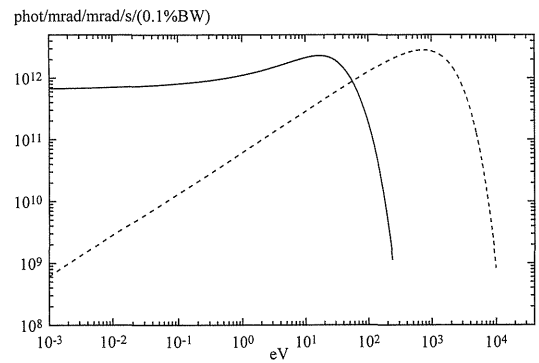


Figure 5. Edge radiation spectrum in the median plane at angular coordinate  $\xi = \gamma^{-1}$  (solid line), as compared with the standard synchrotron radiation (dashed line).

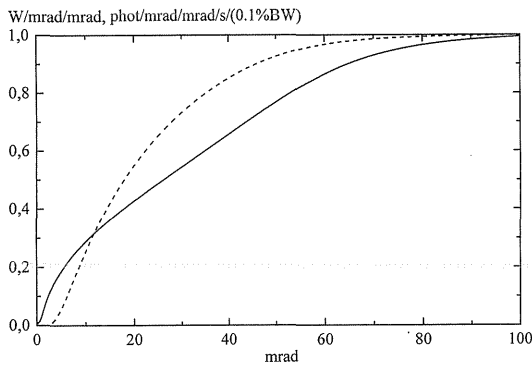


Figure 4. Horizontal distributions of the normalized radiation power-solid line and normalized intensity of photons with critical wavelength-dashed line.

watt/mrad<sup>2</sup>) and intensity of photons with the critical wavelength (in  $phot/mrad^2/s/(0.1\%BW)$ ), computed at the storage ring median plane, are shown. Corresponding simulation of power distribution was based on the Eq. (26). The figure shows that the distributions have no peaks. It follows from the fact that the general amount of synchrotron radiation power is concentrated at short wavelengths, where the ER is not intensive.

The effect of ER peaks is also illustrated by Fig. 5, comparing the radiation spectra in the median plane at a different horizontal angles:  $\xi = \gamma^{-1}$  (ER) and  $\xi \gg \gamma^{-1}$  (standard synchrotron radiation). One can readily see that the ER intensity (in  $phot/mrad^2/s/(0.1\%BW)$ ) falls slower with  $\lambda$  rise and has a ‘softer’ short wavelength tail than the standard synchrotron radiation has.

Fig. 6 shows the two-dimensional angular distribution of the  $\sigma$ -polarized radiation at photon energy 2 eV. As the figure demonstrated, the vertical angular coordinate of the peaks is equal to zero ( $\zeta = 0$ ). The two-dimensional distribution of the  $\pi$ -polarized radiation at 2 eV is shown in Fig. 7. One can see the ER  $\pi$ -component peaks to be located at  $\xi = 0$  and  $\zeta = \pm \gamma^{-1}$ . Both  $\sigma$ - and  $\pi$ -component distributions are symmetric about the electron orbit plane.

One can see the ER to be localized around the straight sec-

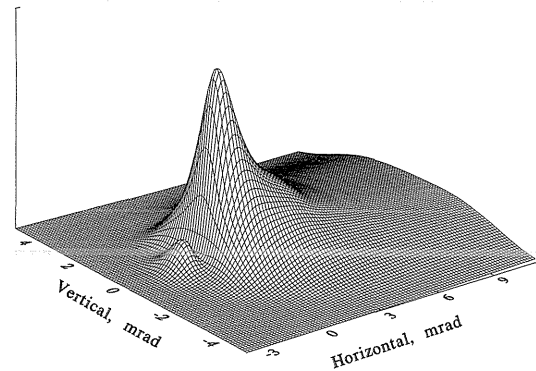


Figure 6. Spatial distribution of  $\sigma$ -polarized edge radiation with 2 eV photon energy.

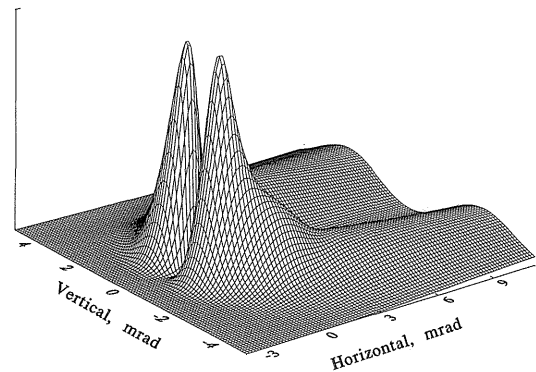


Figure 7. Spatial distribution of  $\pi$ -polarized edge radiation with 2 eV photon energy.

tion axis within a narrow cone of approximately  $4\gamma^{-1}$  angular size, though it is suppressed along the straight section axis, i.e. at  $\xi = 0, \zeta = 0$ . It is worth mentioning that the conventional synchrotron radiation at  $\lambda > \lambda_c$  propagates in a larger vertical angle depending on the wavelength.

Let us consider now the role of interference effects in ER distributions. The results of computation of the interfering ER intensity distribution (in  $phot/mrad^2/s/(0.1\%BW)$ ) on

the detector screen along the horizontal axis for the photons with 2 eV energy are presented at the Fig. 8. In addition to the resulting interfering distribution (solid line), intensity distributions of the radiation from each of the edges individually, as if the other edge was absent, are shown by dashed line in Fig. 8. The resulting intensity distribution in Fig. 8 (solid line) illustrate the interference of the ER generated by single electron at two bending magnet edges bounding the straight gap of the storage ring. The Fig. 9 shows the corresponding two-dimensional intensity distribution for 2 eV photons on the detector screen. One can easily recognize the system of concentric interference rings well-known in optics.

#### 4. Edge radiation in long-wavelength region

In this chapter we will give some approximate formulae which can help one to reveal the mechanism of formation of the electron ER at  $\lambda > \lambda_c$  thus supplementing the computation results presented above. Let us examine the behaviour

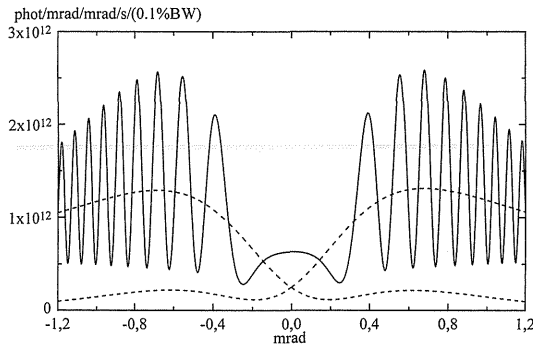


Figure 8. Horizontal distribution of 2 eV interfering edge radiation in the median plane (solid line). The dashed lines show the distributions of radiation corresponding to each bending magnet edge separately.

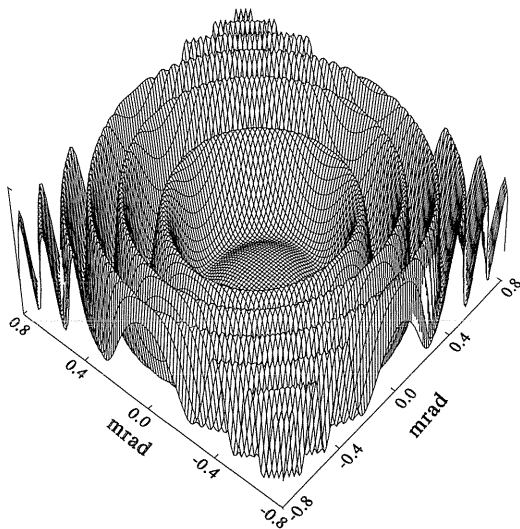


Figure 9. Spatial distribution of  $(\sigma + \pi)$  interfering edge radiation with 2 eV photon energy.

of functions  $F_{\sigma, \pi}(\xi, \zeta)$ , see (21). The approach employed here bear close similarity to those used for the analysis of the 'zero-frequency' radiation properties<sup>16,17</sup>.

Using the integration by parts, one can obtain the following expressions:

$$F_{\sigma}(\xi, \zeta) = \frac{-\gamma\zeta}{1 + \gamma^2(\xi^2 + \zeta^2)} - i \frac{\pi}{\lambda\gamma^2} \int_{y_1}^{\infty} \exp(i\Phi(y)) \times (\gamma\xi - \gamma\beta_x(y)) dy, \quad (27)$$

$$F_{\pi}(\xi, \zeta) = \frac{\gamma\zeta}{1 + \gamma^2(\xi^2 + \zeta^2)} + i \frac{\pi\gamma\zeta}{\lambda\gamma^2} \int_{y_1}^{\infty} \exp(i\Phi(y)) dy. \quad (28)$$

The magnitude  $\rho_0/\gamma$  is the characteristics length unit of the function  $\gamma\beta_x(y)$  changing. Each term of the phase  $\Phi(y)$  in Eq. (20) has his own characteristics length unit (the phase term's variation is of the order of one at this characteristic length unit). The characteristic length units are the following at  $\gamma\xi \leq 1$ ,  $\gamma\zeta \leq 1$ :  $\lambda\gamma^2$  for the first term,  $\sqrt{\lambda\rho_0\gamma}$  and  $\sqrt[3]{\lambda\rho_0^2}$  for the second and third terms respectively, see (14), (15), (20).

Let the characteristic length of magnetic field change at the bending magnet edge be  $l$ . Analysis of Eqs. (20), (27), (28) shows that if the fringe field length  $l$  is much smaller than the smallest length unit of the phase (i.e. the phase change is much less than one in the region  $l$ ), the length  $l$  can be ignored in (20), (27), (28) and the magnetic field can be approximated by the step-function  $\Theta(y)$ :  $h(y) = \Theta(y)$ . It can be found from outlined considerations that this approximation by the step-function is workable in two cases:

$$\begin{cases} l \ll \rho_0\gamma^{-1} \\ l \ll \lambda\gamma^2 \end{cases} \quad (29)$$

or

$$\begin{cases} \rho_0\gamma^{-1} < l \\ \frac{l^3}{20\rho_0^2} \ll \lambda \end{cases} \quad (30)$$

It is worth attention that the system of inequalities (30) may be fulfilled if  $\lambda > \lambda_c$  only.

It should be stressed that the requirement (30) is much weaker than the  $l \ll \rho_0\gamma^{-1}$  one. Usually the first inequality in (30) is always valid for the high-energy electron storage rings. For example, at HiSOR storage ring the electron beam energy is 700 MeV, bending radius  $\rho_0 = 0.87$  m,  $l \approx 0.12$  m (see Fig. 2), that is  $\rho_0\gamma^{-1} = 0.64$  mm and  $(l^3/20\rho_0^2) \approx 0.1$  mm. It means that the step function approximation is suitable for the computation of ER characteristics with wavelength  $\lambda \gg 0.1$  mm only. As a practical matter, in this case the step function approximation is unsuitable even for this long-wavelength radiation because the magnitude  $\lambda\gamma \gg 150$  mm. Usually the storage ring vacuum chamber has a smaller transversal size; that is the conducting walls of vacuum chamber will change significantly the properties of this long-wavelength electromagnetic radiation. So it is necessary to

use the precise formulae obtained in the previous chapter to computation the ER parameters at HiSOR storage ring.

Let us consider the another example, Siberia-2 electron storage ring (Moscow), whose bending magnets have nearly the same fringe field shape as at HiSOR. The beam energy at Siberia-2 storage ring is 2.5 GeV, orbit radius is  $\rho_0 = 19.6$  m in the part of bending magnet with quarter amplitude field,  $l \approx 0.12$  m, that is  $\rho_0 \gamma^{-1} = 4$  mm and  $(l^3/20\rho_0^2) \approx 225$  nm. The step function approximation is suitable for the computation of ER characteristics at Siberia-2 storage ring beginning from VUV region and for more long-wavelength radiation<sup>25)</sup>.

Below in this chapter we will restrict our consideration by the step-function approximation only. Applying this approximation to Eqs. (27) and (28), we have:

$$F_\sigma(\xi, \zeta) = \frac{-\gamma\xi}{1 + \gamma^2(\xi^2 + \zeta^2)} - i\delta p_0 \exp\left[-i\left(\frac{\chi^3}{3} + p\chi\right)\right] \times \int_x^\infty \exp\left[i\left(\frac{u^3}{3} + pu\right)\right] u du, \quad (31)$$

$$F_\pi(\xi, \zeta) = \frac{\gamma\zeta}{1 + \gamma^2(\xi^2 + \zeta^2)} + i\gamma\zeta p_0^2 \exp\left[-i\left(\frac{\chi^3}{3} + p\chi\right)\right] \times \int_x^\infty \exp\left[i\left(\frac{u^3}{3} + pu\right)\right] du, \quad (32)$$

where

$$p_0 = \left(\frac{3\lambda_c}{4\lambda}\right)^{1/3}, \quad p = p_0^2(1 + \gamma^2\zeta^2), \quad \chi = p_0\gamma\xi\delta.$$

The expressions like (31) and (32) were derived and sufficiently detailed analyzed in Ref. 16. The ER peaks are connected with the first term in Eqs. (31) and (32), while the conventional synchrotron radiation is determined by the second one. Actually, at the large horizontal angle  $|\xi| \gg \gamma^{-1}$  and  $\gamma\xi\delta < 0$  the first term both in (31) and (32) is negligible as compared to the second one, which converts to the well-known expression for the conventional synchrotron radiation.

At  $\lambda \gg \lambda_c$ ,  $\gamma|\xi| \approx 1$ ,  $\gamma|\zeta| \approx 1$  the first term prevails in Eqs. (31), (32). Note that both for  $\sigma$ - and for  $\pi$ -components this term is real. Hence the ER is dominantly linear polarized. To be more specific<sup>18,27)</sup>, for the observer placed at the point  $\{x, D, z\}$ , where  $D \gg |x|$ ,  $D \gg |z|$ , the electric field of the received radiation will be parallel to  $\{x, 0, z\}$  direction.

In the  $\lambda \gg \lambda_c$  limit and at the small angles  $\gamma|\xi| \leq 1$ ,  $\gamma|\zeta| \leq 1$  one can obtain a power series in a small parameter  $p_0$  for the functions  $F_{\sigma, \pi}(\xi, \zeta)$ . The first two terms are:

$$F_\sigma(\xi, \zeta) \cong \frac{-\gamma\xi}{1 + \gamma^2(\xi^2 + \zeta^2)} - i\delta p_0 \int_0^\infty u \exp\left(i\frac{u^3}{3}\right) du, \quad (33)$$

$$F_\pi(\xi, \zeta) \cong \frac{\gamma\zeta}{1 + \gamma^2(\xi^2 + \zeta^2)} + i\gamma\zeta p_0^2 \int_0^\infty \exp\left(i\frac{u^3}{3}\right) du, \quad (34)$$

Approximate relations (33) and (34) are in a qualitative

agreement with the computer results obtained in the previous chapter. It may be seen from this relations that the angular positions and widths of ER peaks no longer depend on the radiation wavelength at  $\lambda \gg \lambda_c$ . Using Eqs. (13), (22), (33) and (34), one can derive the following relation for the  $(\sigma + \pi)$ -intensity distribution of ER generated at a single bending magnet BM1 (i.e. in the absence of the second magnet BM2):

$$\frac{dN}{dt} \Rightarrow \frac{ds}{D^2} \left(\frac{d\lambda}{\lambda}\right) \left(\frac{I}{e}\right) \frac{\alpha\gamma^2}{4\pi^2}, \quad (35)$$

at  $\lambda \rightarrow \infty$ ,  $\xi^2 + \zeta^2 = \gamma^{-2}$ , while for the conventional synchrotron radiation

$$\frac{dN}{dt} \Rightarrow 0 \text{ at } \lambda \rightarrow \infty.$$

The horizontal angular asymmetry of the  $\sigma$ -polarized ER in the electron orbit plane is described by the second term in (33) which is proportional to  $p_0$ . Therefore the asymmetry disappears at  $\lambda \rightarrow \infty$ . It could be seen from (34) that the corresponding term is absent in the series for the  $\pi$ -component of ER.

Let us consider the interference effect of the long-wavelength ER. For the sake of simplicity we will consider now the geometry with the observer placed infinitely far from the bending magnets, at least we need  $D \gg L$ . In this case the ER amplitudes, which are generated at the bending magnets BM1 and BM2, are about the same. Using only the leading first terms in (33) and (34), we get from (25):

$$\frac{dN_\sigma}{dt} = \frac{ds}{D^2} \left(\frac{d\lambda}{\lambda}\right) \left(\frac{I}{e}\right) \frac{4\alpha\gamma^2}{\pi^2} \frac{\gamma^2\xi^2}{(1 + \gamma^2\xi^2 + \gamma^2\zeta^2)^2} \times \sin^2 \left[ \frac{\pi L}{2\lambda\gamma^2} (1 + \gamma^2\xi^2 + \gamma^2\zeta^2) \right], \quad (36)$$

$$\frac{dN_\pi}{dt} = \frac{ds}{D^2} \left(\frac{d\lambda}{\lambda}\right) \left(\frac{I}{e}\right) \frac{4\alpha\gamma^2}{\pi^2} \frac{\gamma^2\zeta^2}{(1 + \gamma^2\xi^2 + \gamma^2\zeta^2)^2} \times \sin^2 \left[ \frac{\pi L}{2\lambda\gamma^2} (1 + \gamma^2\xi^2 + \gamma^2\zeta^2) \right]. \quad (37)$$

We can combine two last equations and get a formula for the  $(\sigma + \pi)$ -intensity distribution of the interfering ER:

$$\frac{dN_{\sigma+\pi}}{dt} = \frac{ds}{D^2} \left(\frac{d\lambda}{\lambda}\right) \left(\frac{I}{e}\right) \frac{4\alpha\gamma^2}{\pi^2} \frac{\gamma^2\theta^2}{(1 + \gamma^2\theta^2)^2} \times \sin^2 \left[ \frac{\pi L}{2\lambda\gamma^2} (1 + \gamma^2\theta^2) \right], \quad (38)$$

where  $\theta^2 = \xi^2 + \zeta^2$ . The expression similar to (38) was derived in Ref. 18 under a different model assumptions. Formula (38) shows in an explicit form the cylindrical symmetry of the interfering ER, displaying set of the concentric interference rings. It follows from (38) also that the interfering ER has the highest intensity amplification at the angle  $\theta = \gamma^{-1}$

and at the wavelengths which satisfy the equation  $2L = \lambda\gamma^2(2n-1)$ , where  $n=1, 2, \dots$ . Under this conditions the interfering ER intensity is four time higher than the intensity of radiation generated at the single bending magnet edge. The highest amplification is impossible to achieve at  $\lambda > 2L\gamma^{-2}$ , and in the long-wavelength limit  $\lambda \gg 2L\gamma^{-2}$  the radiation from the adjacent bending magnet edges is suppressed due to destructive interference. The angular width of the interference circular ring with the number  $k \gg 1$  (the angular distance from zero to the next zero in intensity distribution) is equal to

$$\Delta\theta_k = \sqrt{\frac{\lambda}{2Lk}}. \quad (39)$$

Noteworthy is the decreasing of the circle width with its serial number  $k$  increase. This correlates well with the computer simulated results presented above.

By this means, the ER peaks at  $\lambda \gg \lambda_c$  arise in consequence of the sudden change in magnetic field from nil to the constant level. The peaks appear in the case that the effective trajectory region of the radiation formation is larger than the characteristic length of magnetic field change. The standard expressions for the spectral-angular distributions of the conventional synchrotron radiation are inapplicable to the ER description because of the essential difference in the emission conditions of the ER as compared with that of the conventional synchrotron radiation in high-energy electron storage rings.

Completing this chapter, we recall that here (as well as in previous chapters) the ER was discussed in a single-electron approximation, i.e. zero-emittance beam. Finite transverse size and angular divergence of the real electron beam will induce some changes into the ER intensity distribution observed by the experimenter. This problem is briefly discussed in the next chapter.

## 5. Edge radiation and electron beam diagnostics

Real electron beam in a storage ring has the finite transversal sizes  $\sigma_x, \sigma_z$  and angular spread  $\sigma'_x, \sigma'_z$ . When either angular spreads  $\sigma'_x, \sigma'_z$  or magnitudes  $\sigma_x/D, \sigma_z/D$  (where  $D$  is the distance from the first bending magnet to the detector screen, see Fig. 1) exceed the characteristic dimensions of the ER intensity distribution calculated in single-electron approximation, the real distribution differs from that of the single electron. In this regard the single-electron distribution of the ER may be considered as the reference. Its characteristic angular dimensions are the following at  $\lambda > \lambda_c$ : first, the typical angular size of the ER from one fringe field region,  $\gamma^{-1}$ , and second, the angular sizes of the interference rings  $\Delta\theta_k$ ,  $k=1, 2, 3, \dots$ , see relation (39).

The electron beam of modern electron storage rings very often has the angular spread comparable with the typical angular non-uniformity of the ER, mentioned above. At distances appropriate to the actual experimental conditions the typical values of  $\sigma_x/D$  and  $\sigma_z/D$  are also comparable with the characteristic dimensions of the ER intensity distribu-

tion calculated for a single electron.

The fact that the angular width of interference circles decreases with the serial number increase (see Eq. (39) and Figs. 8, 9) is favorable to the sensitivity of diagnostics system based on the ER. Under proper conditions the inner part of the ER intensity distribution may be similar to whose of the single-particle distribution, whereas the outer part is smoothed off. When measuring the ER distribution, it is necessary to use the sufficiently narrow monochromatic filters because the ER distribution pattern is very sensitive to the ER wavelength.

The ER based method of electron beam diagnostics consist of the next steps. Firstly, it is necessary to measure the monochromatic ER intensity distribution (one- or two-dimensional). Secondly, it is necessary to fit this ER distributions by the simulated one, computed under the different parameters of the electron beam. The best fit gives the desired characteristics of real electron beam.

The employment of the ER for the electron beam spread measurements is far more preferable to the use of the conventional synchrotron radiation, which is insensitive to the horizontal divergence and not nearly so sensitive to the vertical divergence of electrons in the beam.

## 6. Summary

The unique features of the edge radiation at  $\lambda > \lambda_c$  in high-energy electron storage rings look very attractive to the users in the spectral range extending from vacuum ultraviolet to far infrared. Indeed, they can expect to get more photons in the spectral range of interest with substantial reduction of the undesirable hard X-ray radiation contribution, i.e. with less thermal damage being caused their optics. The electron beam diagnostics seems to represent another promising application of the edge radiation.

The edge radiation is relatively cheap source. One may use the edge radiation from the straight sections unusable for insertion devices when needed.

## Acknowledgments

I acknowledge with great pleasure the contributions made by my present and former colleagues and co-authors, without whose care and help this work could not be carried out: V. I. Balbekov from IHEP, Protvino, Russia; V. G. Stankevitch and O. V. Chubar from KSRS, Moscow, Russia; A. Hiraya, K. Yoshida and H. Yoshida from Hiroshima University, Japan.

## References

- 1) R. Bossart, J. Bossier, L. Burnod, R. Coisson, E. D'Amico, A. Hofmann and J. Mann: Nucl. Instr. and Meth. **164**, 375 (1979).
- 2) R. Bossart, J. Bossier, L. Burnod, E. D'Amico, G. Ferioli, J. Mann and F. Meot: Nucl. Instr. and Meth. **184**, 349 (1981).
- 3) J. Bossier, L. Burnod, R. Coisson, G. Ferioli, J. Mann and F. Meot: J. Phys. (Paris), Lett. **45**, L343 (1984).
- 4) M. M. Nikitin, A. F. Medvedyev and M. B. Moiseev: Sov. Tech. Phys. Lett. **5**, 347 (1979).
- 5) M. M. Nikitin, A. F. Medvedyev, M. B. Moiseev and V. Ya.

- Epp: *Sov. Phys. JETP* **52**, 388 (1980).
- 6) M. M. Nikitin, A. F. Medvedyev and M. B. Moiseev: *IEEE Trans. Nucl. Sci. NS-28*, 3130 (1981).
  - 7) D. F. Alferov and Yu. A. Bashmakov: *JETP Lett.* **54**, 13 (1981).
  - 8) R. Coisson: *Opt. Commun.* **22**, No. 2, 135 (1977).
  - 9) R. Coisson: *Phys. Rev. A* **20**, 524 (1979).
  - 10) N. V. Smolyakov: *Sov. Phys. Tech. Phys.* **30**, 291 (1985).
  - 11) N. V. Smolyakov: *Sov. Phys. Tech. Phys.* **31**, 741 (1986).
  - 12) N. V. Smolyakov, *Sov. Phys. Tech. Phys.* **33**, 1320 (1988).
  - 13) D. Trbojevic, E. Courant, S. Peggs and A. Hahn: Proceedings of 1998 EPAC Conference, Stockholm, June 22–26, 1623.
  - 14) A. A. Hahn: Proceedings of 1997 PAC Conference, Vancouver, May 12–16.
  - 15) V. G. Bagrov, M. B. Moiseev, M. M. Nikitin and N. I. Fedosov: *Izv. Vuzov, Fizika*, **3**, 26 (1981) (in Russian).
  - 16) V. G. Bagrov, M. B. Moiseev, M. M. Nikitin and N. I. Fedosov: *Nucl. Instr. and Meth.* **195**, 569 (1982).
  - 17) E. G. Bessonov: *Sov. Phys. JETP* **53**, 433 (1981).
  - 18) E. G. Bessonov: *Sov. Phys. Tech. Phys.* **28**, 837 (1983).
  - 19) Yu. A. Bashmakov: *Sov. Phys. Tech. Phys.* **31**, 310 (1986).
  - 20) Yu. A. Bashmakov: *Rev. Sci. Instr.* **63**, 343 (1992).
  - 21) Yu. A. Bashmakov: Proceedings of 1998 EPAC Conference, Stockholm, June 22–26, 565.
  - 22) A. Titov and A. Yarov: *Nucl. Instr. and Meth.* **A308**, 117 (1991).
  - 23) O. V. Chubar and N. V. Smolyakov: 10th International Conference on Vacuum Ultraviolet Radiation Physics (Scientific Program and Abstracts), Paris, July 27–31 (1992).
  - 24) O. V. Chubar and N. V. Smolyakov: *J. Optics (Paris)* **24**, 117 (1993).
  - 25) O. V. Chubar and N. V. Smolyakov: Proceedings of the 1993 IEEE Particle Accelerator Conference, Washington, May 17–20, 1626.
  - 26) R. A. Bosch, T. E. May, R. Reininger and M. A. Green: *Rev. Sci. Instr.* **67**, 3346 (1996).
  - 27) R. A. Bosch: *Nucl. Instr. and Meth. A* **386**, 525 (1997).
  - 28) Y.-L. Mathis, P. Roy, B. Tremblay, A. Nucara, S. Lupi, P. Calvani and A. Gerschel: *Phys. Rev. Lett.* **80**, 1220 (1998).
  - 29) O. Chubar, I. Nagornykh and Y. Krylov: Proceedings of 1994 EPAC Conference, London, June 27–July 1, 1673.
  - 30) N. A. Artemiev, O. V. Chubar and A. G. Valentinov: Proceedings of 1996 EPAC Conference, Barcelona, June 10–14, 340.
  - 31) N. V. Smolyakov, A. Hiraya and H. Yoshida: Proceedings of 1998 APAC Conference, KEK, Tsukuba, March 23–27.
  - 32) N. V. Smolyakov, A. Hiraya and H. Yoshida: Proceedings of 1998 EPAC Conference, Stockholm, June 22–26, 1604.
  - 33) N. V. Smolyakov, H. Yoshida and A. Hiraya: to be published in *Nucl. Instr. and Meth.*
  - 34) G. Muelhaupt and C. Denise: *Nucl. Instr. and Meth. A* **387**, 319 (1997).
  - 35) K.-J. Kim: *Phys. Rev. Lett.* **76**, 1244 (1996).
  - 36) M. Castellano: *Nucl. Instr. and Meth. A* **391**, 375 (1997).
  - 37) V. G. Bagrov, M. M. Nikitin, N. N. Sirota and N. I. Fedosov: *Nucl. Instr. and Meth. A* **282**, 402 (1989).
  - 38) M. Taniguchi and J. Ghijsen: *Syn. Rad. News* **10**, 5 (1997).
  - 39) M. Taniguchi and J. Ghijsen: *J. Syn. Rad.* **5**, 1176 (1998).
  - 40) K. Yoshida, T. Takayama and T. Hori: *J. Syn. Rad.* **5**, 345 (1998).
  - 41) K. Yoshida, M. Andreyashkin, K. Goto, E. Hashimoto, G. Kutluk, K. Matsui, K. Mimura, H. Namatame, N. Ojima, K. Shimada, M. Taniguchi, S. Yagi, I. Endo, T. Takahashi, A. Hiraya, H. Sato, T. Sekitani, K. Tanaka, H. Yoshida, D. Amano, K. Aoki, T. Hori, K. Kawamura, T. Takayama, N. Yasumitsu, T. Ishizuka and H. Morimoto: Proceedings of 1998 APAC Conference, KEK, Tsukuba, March 23–27.
  - 42) R. P. Walker: *Nucl. Instr. and Meth. A* **267**, 537 (1988).